Monthly Notices
of the
ROYAL ASTRONOMICAL SOCIETY

Mon. Not. R. Astron. Soc. **419,** 1721–1726 (2012) doi:10.1111/j.1365-2966.2011.19836.x

Where will supersymmetric dark matter first be seen?

L. Gao,[1,2]★ C. S. Frenk,[2] A. Jenkins,[2] V. Springel[3,4] and S. D. M. White[5]

[1]*Partner Group of the Max Planck Institute for Astrophysics, National Astronomical Observatories, Chinese Academy of Sciences, Beijing 100012, China*
[2]*Institute of Computational Cosmology, Department of Physics, University of Durham, Science Laboratories, South Road, Durham DH1 3LE*
[3]*Heidelberger Institut für Theoretische Studien, Schloss-Wolfsbrunnenweg 35, 69118 Heidelberg, Germany*
[4]*Zentrum für Astronomie der Universität Heidelberg, Astronomisches Recheninstitut, Mönchhofstr. 12-14, 69120 Heidelberg, Germany*
[5]*Max-Planck Institute for Astrophysics, Karl-Schwarzschild Str. 1, D-85748 Garching, Germany*

Accepted 2011 September 14. Received 2011 September 8; in original form 2011 July 7

ABSTRACT

If the dark matter consists of supersymmetric particles, γ-ray observatories such as the Large Area Telescope aboard the *Fermi* satellite may detect annihilation radiation from the haloes of galaxies and galaxy clusters. Much recent effort has been devoted to searching for this signal around the Milky Way's dwarf satellites. Using a new suite of high-resolution simulations of galaxy cluster haloes (the Phoenix Project), together with the Aquarius simulations of Milky Way-like galaxy haloes, we show that higher signal-to-noise ratio and equally clean signals are, in fact, predicted to come from nearby rich galaxy clusters. Most of the cluster emission is produced by small subhaloes with masses less than that of the Sun. The large range of mass scales covered by our two sets of simulations allows us to deduce a physically motivated extrapolation to these small (and unresolved) masses. Since tidal effects destroy subhaloes in the dense inner regions of haloes, most cluster emission is then predicted to come from large radii, implying that the nearest and brightest systems should be much more extended than *Fermi*'s angular resolution limit. The most promising targets for detection are clusters such as Coma and Fornax, but detection algorithms must be tuned to the predicted profile of the emission if they are to maximize the chance of finding this weak signal.

Key words: methods: numerical – galaxies: haloes – dark matter.

1 INTRODUCTION

Annihilation radiation at γ-ray frequencies offers one of the most exciting prospects for non-gravitational detection of cold dark matter (CDM) and is expected if the dark matter consists of supersymmetric particles (e.g. Berezinsky, Bottino & Mignola 1994; Bergström, Ullio & Buckley 1998; Berezinsky, Dokuchaev & Eroshenko 2003; Stoehr et al. 2003; Koushiappas, Zentner & Walker 2004; Colafrancesco, Profumo & Ullio 2007; Diemand, Kuhlen & Madau 2007; Kuhlen, Diemand & Madau 2008; Pieri, Bertone & Branchini 2008; Springel et al. 2008a; Strigari et al. 2008; Jeltema, Kehayias & Profumo 2009; Ackermann et al. 2010; Zavala, Springel & Boylan-Kolchin 2010; Sanchez-Conde et al. 2011). Much effort is being devoted to searching for this signal around the Milky Way's dwarf companions, in particular using the *Fermi* satellite (Abdo et al. 2010).

Predictions for the properties of the annihilation radiation rely on a detailed understanding of the structure of CDM haloes which can be gained only through high-resolution numerical simulations of halo formation. The structure of galaxy-mass CDM haloes has been investigated in considerable depth (e.g. Diemand et al. 2007, 2008; Kuhlen et al. 2008; Springel et al. 2008a,b; Anderson et al. 2010; Kamionkowski, Koushiappas & Kuhlen 2010) showing that the radial distribution of low-mass subhaloes, and thus of annihilation radiation, is much less centrally concentrated than that of the dark matter as a whole. In the Milky Way, this results in the dominant subhalo contribution to the annihilation radiation coming from a large galactrocentric distance and so appearing almost uniform across the sky to an observer on Earth (Springel et al. 2008a). This same effect causes the annihilation radiation from an external galaxy cluster to appear much less centrally concentrated than the distribution of galaxies. As we show below, this has significant implications for the optimal strategy for detecting the annihilation signal.

In this paper, we present some of the largest high-resolution simulations of cluster haloes to date (the Phoenix Project) and use them to investigate the detailed structure of the dark matter distribution in clusters and its halo-to-halo variation. We use these data, together with data from the Aquarius set of galaxy halo simulations (Springel et al. 2008b), to predict the expected γ-ray annihilation radiation from cluster haloes which we compare to

★E-mail: lgao@bao.ac.cn

the expected annihilation radiation from giant and satellite galaxy haloes.

As we were completing this work, Pinzke, Pfrommer & Bergstrom (2011) and Sanchez-Conde et al. (2011) posted preprints investigating, amongst other things, the γ-ray annihilation radiation expected from galaxy clusters. The luminosity and spatial distribution of this radiation depend sensitively on the properties of surviving dark matter subhaloes down to the limiting mass of the CDM power spectrum, which may be in the range 10^{-6} to $10^{-12}\,\mathrm{M}_\odot$ (Hofmann, Schwarz & Stöcker 2001; Green, Hofmann & Schwarz 2005). For their analysis, Pinzke et al. (2011) relied on an extrapolation of scalings based on the published results for simulations of galactic dark matter haloes, including those of the Aquarius Project, while Sanchez-Conde et al. (2011) extended the semi-analytic model of Kamionkowski et al. (2010), rescaling relevant model parameters. Combining the Phoenix and Aquarius simulations, we test explicitly the validity of the scalings used by Pinzke et al. (2011) and Sanchez-Conde et al. (2011), we investigate their underlying physical basis and we thus construct a more robust (though still uncertain) framework for extrapolation. For the most part, our results are in agreement with those of Pinzke et al. (2011), but not with those of Sanchez-Conde et al. (2011) who infer a much weaker contribution from subhaloes to the total annihilation radiation from clusters than that found by Pinzke et al. (2011) or us. In this study, we also present an estimate of the expected signal-to-noise ratio (S/N) of the annihilation radiation from nearby clusters and compare it to that from nearby dwarf and giant galaxies.

The outline of this paper is as follows. Sections 2 and 3 give brief descriptions of our simulation suite and of a model for calculating the annihilation flux and its S/N in an idealized experiment. In Section 4, we discuss our results and their implications for dark matter detection.

2 NUMERICAL SIMULATIONS

The new dark matter simulations analysed in this study come from the Phoenix Project (Gao et al., in preparation). We supplement them with previous high-resolution simulations of galactic haloes from the Aquarius Project carried out by the Virgo Consortium (Springel et al. 2008a,b). Starting from initial conditions appropriate for the ΛCDM cosmology, both sets of simulations integrate the orbits of large numbers of particles using the GADGET-3 N-body code (see Springel et al. 2008a). The cosmological parameters adopted for both the Aquarius and Phoenix projects are those of Virgo's Millennium Simulation (Springel et al. 2005): $\Omega_\mathrm{m} = 0.25$, $\Omega_\Lambda = 0.75$, $\sigma_8 = 0.9$, $n_\mathrm{s} = 1$, and a Hubble constant $H_0 = 100\,h\,\mathrm{km\,s^{-1}} = 73\,\mathrm{km\,s^{-1}\,Mpc^{-1}}$. These were close to the best-fitting values derived from the first year of data from the *Wilkinson Microwave Anisotropy Probe* (*WMAP*) satellite (Spergel et al. 2003) but are not consistent with the parameter ranges found through analysis of the 7-year *WMAP* data together with other large-scale structure observations (Komatsu et al. 2011). The small offset is, however, of no consequence for the topics addressed in this paper.

For the Phoenix Project, we have carried out a suite of extremely high-resolution simulations of the dark matter distribution in galaxy clusters. This suite consists of nine cluster-sized dark matter haloes with masses in the range $[5\text{–}20] \times 10^{14}\,h^{-1}\mathrm{M}_\odot$. These were selected at random from the Millennium Simulation and resimulated at various numerical resolutions. The largest of these 'Phoenix' simulations, labelled Ph-A-1, represents the dark matter with 1.0×10^9 particles within r_{200}, the radius at which the enclosed mean density is 200 times the cosmic critical density. It has a particle mass of $6.4 \times 10^5\,h^{-1}\,\mathrm{M}_\odot$ and a Plummer-equivalent force softening of $0.15\,h^{-1}$ kpc in comoving coordinates at all times. This particular cluster has also been simulated at four lower resolution levels (producing Ph-A-2 to Ph-A-5) in order to assess how resolution affects inferences about cluster structure. At the next-to-highest resolution level ($\sim 1.3 \times 10^8$ particles within r_{200}), we have simulated an additional eight clusters (Ph-B-2 to Ph-I-2) with a particle mass of about $5 \times 10^6\,h^{-1}\,\mathrm{M}_\odot$ and a force softening of $0.32\,h^{-1}$ kpc in order to quantify the cluster-to-cluster variation in dark matter properties. We will present details of the Phoenix simulation suite in a forthcoming paper (Gao et al., in preparation).

3 RESULTS

3.1 The total cluster surface brightness

The total γ-ray annihilation luminosity of a dark matter halo is the sum of contributions from the smooth main halo, from resolved subhaloes and from unresolved subhaloes. [Caustics and tidal streams make a negligible contribution to the annihilation luminosity; Vogelsberger & White (2011).] If the density distribution in the inner regions of the smooth main halo and the resolved subhaloes is assumed to be adequately fitted by the Navarro–Frenk–White (NFW) formula (Navarro, Frenk & White 1996, 1997), their emission integrals $\int \rho^2 \mathrm{d}V$ can be estimated simply as $1.23\,V_\mathrm{max}^4/(G^2 r_\mathrm{max})$ (Springel et al. 2008a). Here V_max is the maximum circular velocity of the halo or subhalo and r_max is the radius at which this maximum circular velocity is reached.

In Fig. 1, we show the azimuthally averaged surface brightness profile for Ph-A-1, split into the components due to the smooth dark matter distribution and to subhaloes resolved down to four mass thresholds differing by factors of 10. The subhalo component is clearly much less centrally concentrated to the cluster centre than the smooth component, and its shape appears independent of mass threshold as far as can be judged given the noise introduced by the finite number of subhaloes involved. The overall level of subhalo emission increases steadily as the threshold decreases. The smallest subhaloes resolved in Ph-A-1 have masses $\sim 5 \times 10^7\,\mathrm{M}_\odot$, well below the masses expected for the haloes of luminous galaxies but far above the lower limit for subhaloes in a ΛCDM universe which could be as low as $10^{-12}\,\mathrm{M}_\odot$ (Hofmann et al. 2001; Bertone, Hooper & Silk 2005). Considerable extrapolation is thus necessary in order to estimate the total subhalo emission. Note that even at the Ph-A-1 resolution threshold of $5 \times 10^7\,\mathrm{M}_\odot$, the surface brightness is dominated by the subhalo component at radii greater than 200 kpc.

To calibrate the extrapolation to lower subhalo masses, we combine results from our nine Phoenix simulations with results from six higher resolution simulations of galaxy haloes from the Aquarius Project (Springel et al. 2008a,b). Fig. 2 shows the total annihilation luminosity per unit halo mass (M_{200}) and per decade in subhalo mass from subhaloes with masses ranging over seven orders of magnitude, from 10^5 to $10^{12}\,\mathrm{M}_\odot$. In the overlap region between 10^8 and $10^9\,\mathrm{M}_\odot$, the Phoenix and Aquarius results agree to about 30 per cent. This is within the scatter expected, given the finite number of realizations (illustrated by the shaded area) and the roll-off as subhalo mass approaches 1 per cent of the parent mass. Well away from these cut-offs, the shape of this curve is very similar to that of the halo luminosity per unit mass expected for the Universe as a whole, shown as the dashed magenta curve in Fig. 2. This reflects the fact that the luminosity is dominated by subhaloes in the outer regions which were accreted recently (Gao et al. 2004) and so have similar luminosities and abundance per unit mass (apart from

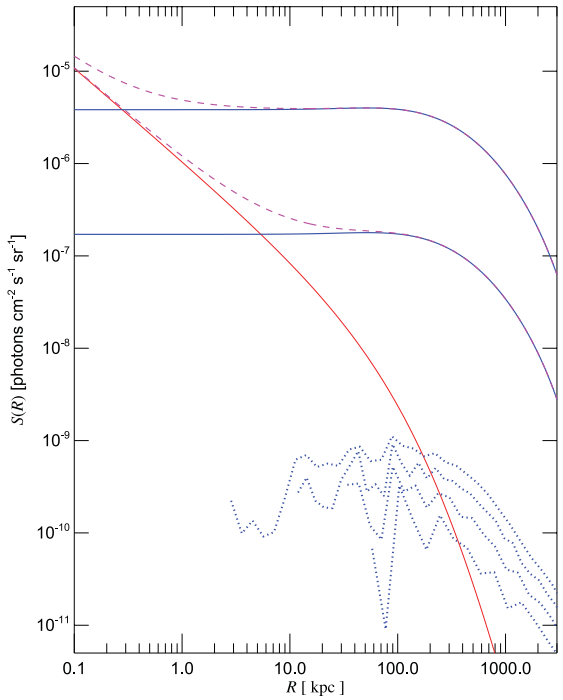

Figure 1. Surface brightness profiles from dark matter annihilation for various components of the Ph-A-1 simulation of a rich galaxy cluster. Surface brightness is given in units of annihilation photons cm^{-2} s^{-1} sr^{-1} for fiducial values of 100 GeV for $m_{\rm p}$, the dark matter particle mass, and 3×10^{-26} cm^3 s^{-1} for $\langle \sigma v \rangle$, the thermally averaged velocity-weighted annihilation cross-section, assuming $N_\gamma = 1$ photons per annihilation. This surface brightness scales as $N_\gamma \langle \sigma v \rangle / m_{\rm p}^2$. Projected radius is given in units of kpc. The red line shows radiation from the smoothly distributed dark matter within the main component of the cluster. The ragged blue dotted lines show radiation from resolved dark matter subhaloes with masses exceeding 5×10^7, 5×10^8, 5×10^9 and 5×10^{10} M$_\odot$ (from top to bottom). Extrapolating to mass limits of 10^{-6} and 10^{-12} M$_\odot$ as discussed in the text gives rise to the smooth blue curves. The purple dashed lines show the results of summing smooth and subhalo contributions.

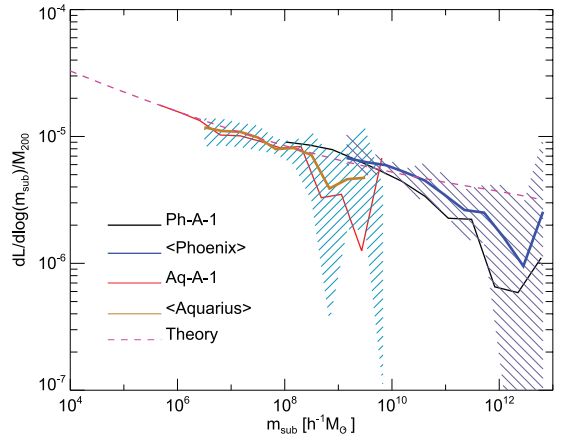

Figure 2. Annihilation luminosity (in arbitrary units) from subhaloes lying within r_{200} per decade in subhalo mass and per unit halo mass (M_{200}) for the Phoenix and Aquarius simulations. The level 1 simulations are shown by the black (Phoenix) and red (Aquarius) lines and the medians of the nine Phoenix and six Aquarius level 2 simulations by the thick blue and orange lines, respectively. The full scatter in each set of simulations is indicated by the shaded areas. The dashed magenta line gives the predicted annihilation luminosity density per decade in halo mass from the cosmic population of dark matter haloes.

a small bias correction of 1.5) as the haloes in a representative volume of the Universe. Thus, we can use analytic predictions for the abundance and concentration of field haloes (Sheth & Tormen 2002; Neto et al. 2007) to extrapolate our simulation results to much lower subhalo masses. The upper blue curves in Fig. 1 show the resulting predictions for minimum subhalo masses of 10^{-6} and 10^{-12} M$_\odot$, respectively. The most uncertain part of this extrapolation is the assumption that halo concentration continues to increase towards lower masses in the same way as measured over the mass range simulated so far. This assumption has not yet tested explicitly and has a very large effect on the results. For example, if all (sub)haloes less massive than 10^5 M$_\odot$ are assumed to have similar concentration, then the total predicted emission from subhaloes would be more than two orders of magnitude below that plotted in Fig. 1 for an assumed cut-off mass of 10^{-6} M$_\odot$.

With our adopted concentration scaling, subhaloes dominate the surface brightness beyond projected radii of a few kiloparsecs, as may be seen in Fig. 1. Surface brightness is almost constant between 10 and 300 kpc, dropping by a factor of 2 only at 460 kpc. At the virial radius of the cluster ($r_{200} = 1936$ kpc), the surface brightness of the subhalo component is a factor of 14 below its central value. Within this radius the luminosity from resolved subhaloes in Ph-A-1 is more than twice that from the smooth halo, even though these subhaloes account only for 8 per cent of the mass. Extrapolating to minimum subhalo masses of 10^{-6} and 10^{-12} M$_\odot$, the subhalo excess becomes 718 and 16 089, respectively. These boost factors substantially exceed the equivalent factors predicted for the galaxy haloes of the Aquarius Project. This is because of the additional high-mass subhaloes which contribute in the cluster case (see Fig. 2) together with the lower concentration of cluster haloes relative to galaxy haloes, which reduces the emission from the smooth component. Note that the boost factor for Aq-A-1 obtained with the extrapolation we use here is smaller by a factor of 2.4 than the value quoted in Springel et al. (2008a).

For the resolved component, there is significant variation amongst the nine Phoenix haloes, but the median value of the total boost factor (for a cut-off mass of 10^{-6} M$_\odot$) is 1125, which, for the reasons just given, is about 12 times the median boost factor we obtain by applying the same method to the Aquarius haloes. Comparing these results suggests that the ratio of subhalo to smooth main halo luminosity within r_{200} (subhalo 'boost factor') varies with halo mass approximately as

$$b(M_{200}) = L_{\rm sub}/L_{\rm main} = 1.6 \times 10^{-3} (M_{200}/{\rm M}_\odot)^{0.39}. \quad (1)$$

The total luminosity of a halo is therefore $L_{\rm tot} = (1 + b)L_{\rm main}$, where $L_{\rm main}$ is the emission of the smooth halo. In addition, the projected luminosity profile of the subhalo component can be well approximated by

$$S_{\rm sub}(r) = \frac{16 b(M_{200}) L_{\rm main}}{\pi \ln(17)} \frac{1}{r_{200}^2 + 16 r^2}. \quad (2)$$

These formulae will be used to estimate dark matter annihilation luminosities and surface brightness profiles for haloes with different masses in subsequent sections.

3.2 Surface brightness and signal to noise ratio of galaxies and clusters

Putting together results from the Phoenix and Aquarius projects, we can assess the relative ease of detection of cluster, galaxy and dwarf satellite haloes. In the left-hand panel of Fig. 3, we show predicted

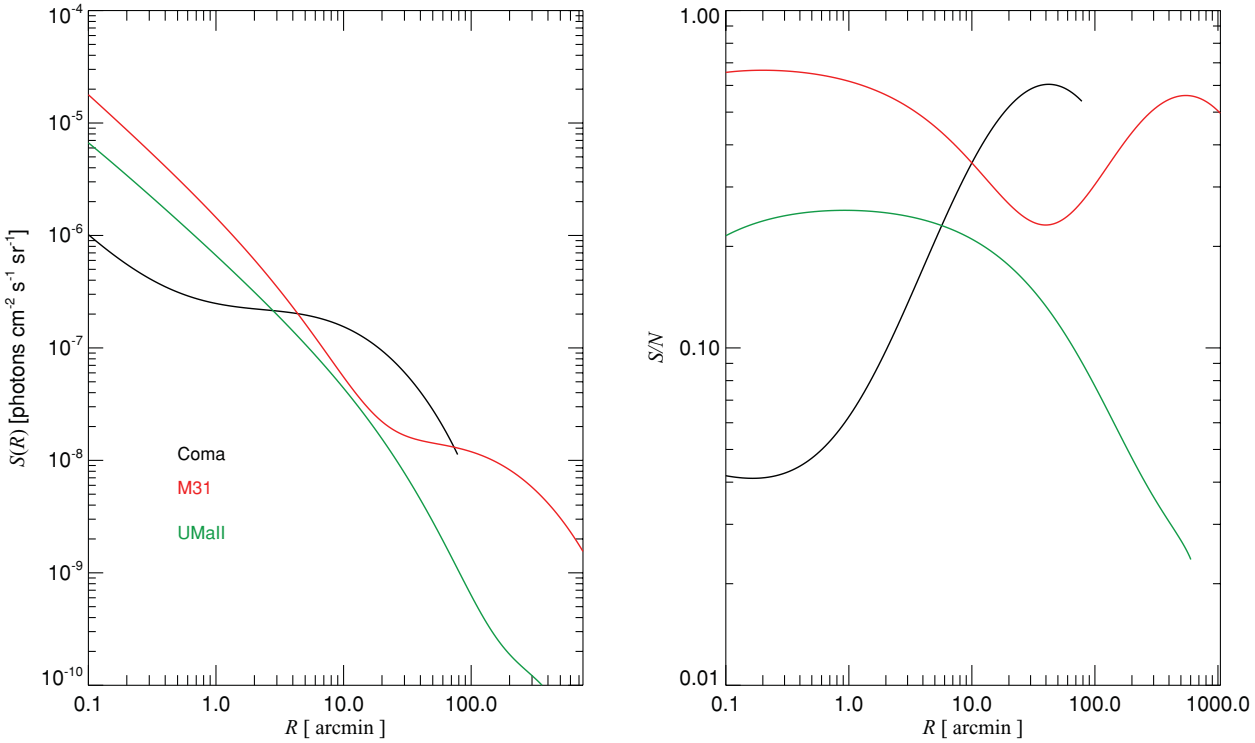

Figure 3. Left-hand panel: predicted surface brightness profiles of annihilation radiation (in units of annihilation photons cm^{-2} s^{-1} sr^{-1}) for a dwarf galaxy (UMa-II; green line), for the nearest large galaxy (M31; red line) and for a rich galaxy cluster (the Coma cluster; black line). As in Fig. 1, surface brightness scales as $N_\gamma \langle \sigma v \rangle / m_{\rm p}^2$. Projected radius is given in arcminutes. The inner steeply rising part of each curve is due to smoothly distributed dark matter in the main halo, while the shoulder of extended emission is produced by low-mass subhaloes. Each profile is truncated at r_{200}, the nominal radius of the dark matter halo. Right-hand panel: estimates of the S/N within a circular aperture of radius R (in arcminutes). The signal is obtained by direct integration of the corresponding curves in the left-hand panel and the noise is obtained as discussed in the text. S/N scales as $N_\gamma\, B^{-1/2} \langle \sigma v \rangle / m_{\rm p}^2$, where B is the surface brightness of the background, assumed to be uniform.

surface brightness profiles for three of the most promising candidates, the Coma cluster of galaxies, the Andromeda nebula (M31) and the dwarf satellite galaxy, Ursa Major-II (UMa-II), assuming a minimum subhalo mass of $10^{-6}\,{\rm M}_\odot$. We represent Coma and M31 by scaling Ph-A-1 and Aq-A-1 to the appropriate virial masses, $M_{200} = 1.3 \times 10^{15}\,{\rm M}_\odot$ for Coma (Reiprich & Böhringer 2002) and $1.8 \times 10^{12}\,{\rm M}_\odot$ for M31 (Li & White 2008). We model UMa-II as in Springel et al. (2008a) (including the contribution from substructures – the 'subsub' component). At projected radii below 2 arcmin, M31 is about twice as bright as UMa-II and both are substantially brighter than Coma. However, at 20 arcmin the surface brightness of Coma exceeds that of M31 by a factor of 4 and that of UMa-II by about a factor of 6. Beyond about 70 arcmin, M31 is again the brightest object.

For γ-ray telescopes like the *Fermi* Large Area Telescope (*Fermi*-LAT), the detectability of extended objects depends on their contrast relative to the diffuse background. As a simple indicator of S/N, in the right-hand panel of Fig. 3 we estimate the signal within a circular aperture from the enclosed luminosity, and the noise as the square root of the background counts, assumed to be BAt, where B is the background count rate per unit area, A is the area of the aperture in arcmin^2 and t is the exposure time. (This assumes that the background is uniform and larger than the signal, which may not be the case for the smallest apertures.) For the dwarf galaxy UMa-II, the effective S/N is almost independent of aperture for radii less than 10 arcmin, but drops dramatically at larger radii. In contrast, the S/N for Coma rises steeply with increasing aperture to a peak at a radius of about 30 arcmin, significantly larger than the few arcmin resolution of the *Fermi*-LAT at energies $\sim$10 GeV. For M31, the effective S/N has a minimum on this scale and has maxima on scales of 1 and 300 arcmin. In this simple set-up, the maximum achievable S/N ratios for Coma and M31 exceed that for UMa-II by about a factor of 3.

In practice, realistic experiments will find it difficult to achieve these theoretical S/N values for very large apertures. Systematic effects due to variable backgrounds and difficulties in masking bright sources make background correction significantly easier for small apertures. M31 is a particularly difficult case because of its very large angular size, low galactic latitude and confusion from other γ-ray sources in its inner regions. The Coma cluster is significantly more promising because it lies close to the North Galactic Pole and appears 10 times smaller on the sky. On the other hand, an overly small aperture, corresponding for example to the few arcmin resolution of the *Fermi*-LAT instrument at about 10 GeV, would miss a large fraction of the signal in Coma and other nearby galaxy clusters. For a uniform background, the optimal filter has a shape similar to the predicted profile (Springel et al. 2008a) shown in Fig. 3 and represented by equation (2).

4 DISCUSSION AND CONCLUSION

In Table 1, we summarize properties of some nearby astronomical objects which are relevant for the detectability of their dark matter annihilation signal. We consider six galaxy clusters which were already analysed by the *Fermi* collaboration (Ackermann et al. 2010),

Table 1. Principal properties of nearby galaxy clusters, prominent satellites of the Milky Way and the Andromeda nebula, M31. The annihilation luminosity, L, is given in units of the luminosity from the smooth component of the main Aq-A halo, which we use as a proxy for the Milky Way. The observed flux, F, is expressed relative to the flux received by an observer placed 8 kpc from the centre of Aq-A. Similarly, the predicted S/N for an optimal filter placed on each object is normalized to the S/N predicted for a similar filter tuned to the diffuse emission of Aq-A seen from this observer location. For the S/N calculations, we use the optimal filter of Springel et al. (2008a) assuming the background to be the same everywhere and to dominate the signal in all objects.

Object name	Half-light radius (arcmin)	Distance (Mpc)	M_{200} ($M_\odot$)	L ($L_{\rm mw}$)	$F = L/(4\pi d^2)$ ($F_{\rm mw}$)	S/N [$(S/N)_{\rm mw}$]
AWM 7	35.5	67.0	4.2×10^{14}	7.1×10^{4}	3.2×10^{-4}	6.8×10^{-3}
Fornax cluster	84.1	17.5	1.0×10^{14}	1.2×10^{4}	8.0×10^{-4}	7.3×10^{-3}
M49	59.6	18.2	0.4×10^{14}	3.9×10^{3}	2.4×10^{-4}	3.1×10^{-3}
NGC 4636	52.6	17.4	0.24×10^{14}	2.1×10^{3}	1.4×10^{-4}	2.0×10^{-3}
Centaurus (A3526)	40.1	50.5	2.6×10^{14}	3.9×10^{4}	3.1×10^{-4}	5.8×10^{-3}
Coma	36.1	95.8	1.3×10^{15}	2.9×10^{5}	6.4×10^{-4}	1.3×10^{-2}
Draco	16.4	0.082	N/A	5.2×10^{-3}	1.6×10^{-5}	6.3×10^{-4}
UMa-I	18.4	0.066	N/A	4.3×10^{-3}	2.0×10^{-5}	7.5×10^{-4}
LeoI	4.4	0.25	N/A	3.5×10^{-3}	1.2×10^{-6}	8.2×10^{-5}
Fornax dwarf	5.9	0.138	N/A	2.0×10^{-3}	2.2×10^{-6}	1.5×10^{-4}
LeoII	2.5	0.205	N/A	8.5×10^{-4}	4.1×10^{-7}	3.1×10^{-5}
Carina	4.6	0.101	N/A	7.1×10^{-4}	1.4×10^{-6}	1.0×10^{-4}
Sculpt	13.2	0.079	N/A	3.2×10^{-3}	1.0×10^{-5}	4.9×10^{-4}
Sext	3.3	0.086	N/A	3.0×10^{-4}	8.3×10^{-7}	6.1×10^{-5}
UMa-II	28.8	0.032	N/A	2.6×10^{-3}	5.2×10^{-5}	1.3×10^{-3}
Comber	15.9	0.044	N/A	1.6×10^{-4}	1.7×10^{-5}	6.8×10^{-4}
WilI	17.7	0.066	N/A	3.9×10^{-3}	1.8×10^{-5}	7.0×10^{-4}
LMC	82.5	0.049	N/A	3.8×10^{-2}	3.3×10^{-4}	3.1×10^{-3}
SMC	45.5	0.061	N/A	1.9×10^{-2}	1.1×10^{-4}	1.8×10^{-3}
M31	351.5	0.807	1.8×10^{12}	1.3×10^{2}	4.2×10^{-3}	9.3×10^{-3}

13 of the known dwarf satellites of our Galaxy and the nearest giant galaxy, M31.

For the galaxy clusters, distances were taken from the NASA/IPAC Extragalactic Database[1] and virial masses, M_{200} (based on X-ray data), from Reiprich & Böhringer (2002). Values for $V_{\rm max}$ and $r_{\rm max}$ were derived assuming an NFW density profile (Navarro et al. 1996, 1997) and the mass–concentration relation of Neto et al. (2007). We have verified that this relation is consistent with our simulation data down to the resolution limit of Aq-A-1, which is about $10^5\,{\rm M}_\odot$.

Data for dwarf satellites were taken from the mass models of Peñarrubia, Navarro & McConnachie (2008). Their γ-ray luminosities are estimated from an emission integral based on the NFW formula, $\int \rho^2 {\rm d}V = 1.23\,V_{\rm max}^4/(G^2 r_{\rm max})$. As discussed in Springel et al. (2008a), the annihilation signal due to substructures within Milky Way dwarfs (the 'subsub' component) is less than that due to the smooth component of their haloes in almost all cases, so we do not consider it here. The distance of M31 was also taken from the NASA/IPAC Extragalactic Database. We base structural parameters for the M31 halo on the Aq-A-1 simulation which has a very similar mass (Li & White 2008).

We estimate a 'best case' S/N for each object using the optimal filter discussed by Springel et al. (2008a) and assuming a uniform background across the whole sky which dominates the signal in all objects. In this case, the optimal filter has the same shape as the signal, and the S/N can be written in the generic form

$$\mathrm{S/N} = f_{\rm shape}(\theta_{\rm h}/\theta_{\rm psf}) \left[\frac{t\,A_{\rm eff}}{B}\right]^{1/2} \frac{F}{\left(\theta_{\rm h}^2 + \theta_{\rm psf}^2\right)^{1/2}}, \quad (3)$$

where $F = L/(4\pi d^2)$ is the photon flux, $\theta_{\rm h}$ is the half-light radius, $\theta_{\rm psf}$ ($\simeq$10 arcmin for *Fermi* at the relevant energies; Michelson 2007) describes the point spread function of the instrument, t is the integration time, $A_{\rm eff}$ is the effective collecting area of the telescope and B is the background count rate per unit solid angle. The function $f_{\rm shape}(x)$ encodes the detailed shape of the emission profile of the signal (Springel et al. 2008a); it is of order unity and depends only weakly on the ratio $x = \theta_{\rm h}/\theta_{\rm psf}$.

Using the techniques discussed above, we can compare the apparent γ-ray luminosities and achievable S/N ratios for galaxy clusters with those estimated by Springel et al. (2008a) for dwarf satellites of the Milky Way. Results are shown in the Table 1. We find that the brightest nearby cluster, Fornax, is predicted to appear 15 times more luminous than the brightest dwarf spheroidal, UMa-II, and 40–50 times more luminous than UMa-I, Draco or the ultrafaint satellite, Wilman 1. However, the Fornax cluster is quite extended on the sky, and, as a result, when optimal filters are used, the slightly fainter but more compact Coma cluster has a predicted S/N ratio 1.8 times larger and 10 times that of the most easily detectable dwarf spheroidal, UMa-II. Although the Andromeda nebula is predicted to have a comparable S/N, it is not a promising target because of the difficulty in correcting for foreground and other sources of emission. Note that the S/N predicted for both objects is still very small compared to that of the main component of the Milky Way's

[1] http://nedwww.jpac.caltech.edu/

smooth halo. Here also, of course, the main problem is in separating annihilation radiation from other γ-ray signals.

The Coma cluster thus offers an order of magnitude better opportunity than any Milky Way satellite for detecting dark matter or placing limits on its annihilation cross-section. As we have shown, for a high-resolution experiment like *Fermi*, the sensitivity for detecting such radiation will be enhanced by use of a filter which is properly matched to the expected extent of the object. For example, for the optimal filter, the S/N expected for Coma is about 1.5 times higher than the S/N for a filter based on the point spread function of the *Fermi*-LAT, assuming 10 arcmin for the latter at the relevant energies. Detecting annihilation radiation from the Coma or Fornax clusters or placing robust and stringent upper limits will also require careful subtraction of astrophysical sources and an accurate estimate of the background.

ACKNOWLEDGMENTS

We thank the Supercomputer Center of the Chinese Academy of Science, where the simulations were carried out. LG acknowledges support from the one-hundred-talents programme of the Chinese Academy of Science (CAS), the national basic research programme of China (973 programme under grant no. 2009CB24901), the NSFC grants programme (no. 10973018), the Partner Group programme of the Max Planck Society and an STFC Advanced Fellowship, as well as the hospitality of the Institute for Computational Cosmology in Durham, UK. CSF acknowledges a Royal Society Wolfson Research Merit Award and ERC Advanced Investigator grant COSMIWAY. This work was supported in part by an STFC rolling grant to the ICC.

REFERENCES

Abdo A. A. et al., 2010, ApJ, 712, 147
Ackermann M. et al., 2010, J. Cosmol. Astropart. Phys., 5, 25
Anderson B., Kuhlen M., Diemand J., Johnson R. P., Madau P., 2010, ApJ, 718, 899
Berezinsky V., Bottino A., Mignola G., 1994, Phys. Lett. B, 325, 136
Berezinsky V., Dokuchaev V., Eroshenko Y., 2003, Phys. Rev. D, 68, 103003
Bergström L., Ullio P., Buckley J. H., 1998, Astropart. Phys., 9, 137
Bertone G., Hooper D., Silk J., 2005, Phys. Rep., 405, 279
Colafrancesco S., Profumo S., Ullio P., 2007, Phys. Rev. D, 75, 023513
Diemand J., Kuhlen M., Madau P., 2007, ApJ, 657, 262
Diemand J., Kuhlen M., Madau P., Zemp M., Morre B., Potter B., Stadel J., 2008, Nat, 454, 735
Gao L., White S. D. M., Jenkins A., Stoehr F., Springel V., 2004, MNRAS, 355, 819
Green A. M., Hofmann S., Schwarz D. J., 2005, J. Cosmol. Astropart. Phys., 8, 3
Hofmann S., Schwarz D. J., Stöcker H., 2001, Phys. Rev. D, 64, 083507
Jeltema T. E., Kehayias J., Profumo S., 2009, Phys. Rev. D, 80, 2, 023005
Kamionkowski M., Koushiappas S. M., Kuhlen M., 2010, Phys. Rev. D, 81, 043532
Komatsu E. et al., 2011, ApJS, 192, 18
Koushiappas S. M., Zentner A. R., Walker T. P., 2004, Phys. Rev. D, 69, 043501
Kuhlen M., Diemand J., Madau P., 2008, ApJ, 686, 262
Li Y.-S., White S. D. M., 2008, MNRAS, 384, 1459
Michelson P. F., 2007, in Ritz S., Michelson P., Meegan C. A., eds, AIP Conf. Ser. Vol. 921, The First GLAST Symposium. Am. Inst. Phys., New York, p. 8
Navarro J. F., Frenk C. S., White S. D. M., 1996, ApJ, 462, 563
Navarro J. F., Frenk C. S., White S. D. M., 1997, ApJ, 490, 493
Neto A. F. et al., 2007, MNRAS, 381, 1450
Peñarrubia J., Navarro J. F., McConnachie A. W., 2008, ApJ, 673, 226
Pieri L., Bertone G., Branchini E., 2008, MNRAS, 384, 1627
Pinzke A., Pfrommer C., Bergstrom L., 2011, preprint (arXiv:1105.3240)
Reiprich T. H., Böhringer H., 2002, ApJ, 567, 716
Sanchez-Conde M. A., Cannoni M., Zandanel F., Gomez M. E., Prada F., 2011, preprint (arXiv:1104.3530)
Sheth R. K., Tormen G., 2002, MNRAS, 329, 61
Spergel D. N. et al., 2003, ApJS, 148, 175
Springel V. et al., 2005, Nat, 435, 629
Springel V. et al., 2008a, Nat, 456, 73
Springel V. et al., 2008b, MNRAS, 391, 1685
Stoehr F., White S. D. M., Springel V., Tormen G., Yoshida N., 2003, MNRAS, 345, 1313
Strigari L. E. et al., 2008, ApJ, 678, 614
Vogelsberger M., White S. D. M., 2011, MNRAS, 413, 1419
Zavala J., Springel V., Boylan-Kolchin M., 2010, MNRAS, 405, 593

This paper has been typeset from a TEX/LATEX file prepared by the author.